Journal of Sound and Vibration (1995) **185**(5), 791–808

METHOD OF IMAGES FOR THE HARMONIC RESPONSE OF BEAMS AND RECTANGULAR PLATES

R. Gunda, S. M. Vijayakar and R. Singh

Acoustics and Dynamics Laboratory, Department of Mechanical Engineering, The Ohio State University, Columbus, Ohio 43210-1107, *U.S.A.*

(*Received* 9 *June* 1994, *and in final form* 15 *August* 1994)

The feasibility of calculating the narrow band harmonic response of thin plates and beams by using the method of images or the ray tracing technique is examined. The fundamental solution of an infinite plate is employed, in conjunction with appropriately placed images, to obtain the dynamic compliance spectra of simply supported rectangular plates over a wide range of frequencies. Predictions yielded by the method of images are in excellent agreement with the normal mode expansion technique. Simply supported beams are analyzed first by considering the fundamental solution of an infinite beam, and second as a case of a narrow plate with simply supported and roller boundary conditions. Both approaches match well with the closed form solutions and with measurements conducted on two beams. Several issues including convergence characteristics and high frequency behavior are discussed.

1. INTRODUCTION

The method of images or ray tracing techniques have been commonly employed in disciplines such as acoustics, optics and electro-magnetics [1, 2]. However, this method has not been adequately extended to structural vibrations. The only exception seems to be the work on the regions of enhanced responses on strings or thin plates when excited by random loads [3–7]. For instance, Crandall *et al*. [3–5] and Lee [6] have obtained the frequency response of a finite string when excited by a point load whose time history was a wide-band random process. Their image sum method was further extended to calculate the zones of intensified response on a simply supported rectangular plate that was excited by random point forces. Langley and Taylor [7] have analyzed the same problems by using the reverberant field method. Cremer and Heckl [8] have presented a wave cycle closure principle but it has been applied to satisfy the boundary conditions in the thickness direction of a plate. To the best of our knowledge, no other researcher has attempted to calculate the narrow-band harmonic response of thin plates and beams using the method of images. This paper attempts to fill this void.

As a second motivation for our work, we consider the issue of narrow-band harmonic analysis at very high frequencies. We drew inspiration from work in optics and electro-magnetics [2] where researchers routinely work in the regime of wavelengths which are orders of magnitude smaller than the geometrical dimensions of the zone of interest. Consequently, the intent of the work described in this paper is to examine if the use of ray tracing as an underlying mathematical model can conceptually lead to numerical methods capable of predicting narrow-band behavior at very high frequencies which are robust,

0022–460X/95/350791 + 18 $12.00/0

accurate and efficient. Only simple geometries with a few classical boundary conditions are considered.

2. PROBLEM FORMULATION

2.1. PLATE EQUATIONS

Let Ω_-, Ω_+, $\partial\Omega$ be the interior domain, exterior domain and the boundary of the plate, respectively. Assume the boundary $\partial\Omega$ is sufficiently smooth. According to classical theory [9], the equation governing the flexural vibration of an isotropic, homogeneous plate of constant thickness h is expressed in terms of transverse displacement w as

$$D\nabla^4 w(\vec{r}_0, t) + \rho h \frac{\partial^2 w(\vec{r}_0, t)}{\partial t^2} = p(\vec{r}_s, t), \tag{1}$$

where $D = Eh^3/12(1-\nu^2)$ is the flexural rigidity of the plate; further, ∇^4, t, E, ρ, p and ν are the biharmonic operator, time, Young's modulus of the material of the plate, density, lateral force per unit area and the Poisson ratio, respectively. Source and observation (response) points are given by position vectors $\vec{r}_s$ and $\vec{r}_0$, respectively, both within Ω_-. At a regular point on the boundary $\partial\Omega$, bending moment $M_n(w)$, twisting moment $M_t(w)$ and shear force $V_n(w)$ are given as follows, where α is the angle from the x-axis to the outer normal and $\mathrm{d}/\mathrm{d}n$, $\mathrm{d}/\mathrm{d}s$ denote the normal and tangential derivatives, respectively, on $\partial\Omega$. (Definitions of the symbols used in this paper are given in Appendix A)

$$M_n(w) = \frac{D}{2}\left\{-(1+\nu)\nabla^2 w + (1-\nu)\left[\left(\frac{\partial^2 w}{\partial y^2} - \frac{\partial^2 w}{\partial x^2}\right)\cos 2\alpha - 2\frac{\partial^2 w}{\partial x\,\partial y}\sin 2\alpha\right]\right\}, \tag{2}$$

$$M_t(w) = -\frac{D(1-\nu)}{2}\left\{\left(\frac{\partial^2 w}{\partial y^2} - \frac{\partial^2 w}{\partial x^2}\right)\sin 2\alpha + 2\frac{\partial^2 w}{\partial x\,\partial y}\cos 2\alpha\right\}, \tag{3}$$

$$V_n(w) = -D\frac{\mathrm{d}}{\mathrm{d}n}(\nabla^2 w) + \frac{\mathrm{d}}{\mathrm{d}s}M_t(w). \tag{4}$$

Assume harmonic excitation at a circular frequency ω,

$$p(\vec{r}_s, t) = F(\vec{r}_s)\exp(\mathrm{i}\omega t). \tag{5}$$

The resulting steady state response w is given by

$$w(\vec{r}_0, t) = u(\vec{r}_0)\exp(\mathrm{i}wt). \tag{6}$$

Substituting equation (6) in equation (1), the governing equation can be expressed in terms of the frequency parameter λ as follows. From this point on, only the spectral domain is considered in terms of $u(\vec{r}_0)$ and $F(\vec{r}_s)$:

$$(\nabla^4 - \lambda^4)u(\vec{r}_0) = \frac{F(\vec{r}_s)}{D}, \qquad \lambda^4 = \rho h\omega^2/D. \tag{7}$$

To solve the plate vibration problem, the biharmonic equation has to be solved subject to various boundary conditions on the plate edge. In this paper, the discussion is limited to rectangular plates with simply supported or roller boundary conditions. Structural

damping behavior will be considered by replacing D with $\bar{D} = D(1+i\eta)$, where η is the loss factor.

2.2. FUNDAMENTAL SOLUTION

The following fundamental solution $U(\vec{r}_0, \vec{r}_s, \lambda)$ to equation (7) represents the transverse deflection of an infinite plate at a point $\vec{r}_0$ due to a unit concentrated load at a point $\vec{r}_s$ of frequency ω [10]:

$$U(\vec{r}_0, \vec{r}_s, \lambda) = -\frac{i}{8\lambda^2 D}\,[H_0^1(\lambda r) - H_0^1(i\lambda r)], \tag{8}$$

where $r = |\vec{r}_0 - \vec{r}_s|$ is the distance between the source point and the observation point and H_0^1 is the zero order Hankel function of the first kind. It has been used by Niwa *et al*. [11] to develop a boundary element formulation for bending vibrations of plates. This fundamental solution satisfies the Sommerfeld radiation condition, which implies that only the waves travelling away from the source are considered [12].

2.3. SEMI-INFINITE PLATE

The fundamental solution given by equation (8) is based on the assumption that the plate is infinite. To apply this to a finite plate, the boundary conditions on the plate edge have to be satisfied. The method of images is essentially a scheme for satisfying the boundary conditions for a finite plate.

Let us obtain the solution for a semi-infinite plate subjected to a point force F at point $r_s(x_s, y_s)$, as shown in Figure 1. Along the edge of the plate, boundary conditions are satisfied by placing a fictitious point force F' at a distance y_s from the edge which is equal to the distance of F from the edge of the plate. Depending on the magnitude of F', certain boundary conditions can be satisfied along the edge of the plate. Let $r_a(x, 0)$ be any point on the edge of the semi-infinite plate in accordance with Figure 1. The co-ordinates of the source and image points are $r_s(x_s, y_s)$ and $r_i(x_i, y_i)$. Since these points are mirror images of each other about the edge line ($y = 0$), $x_s = x_i$ and $y_i = -y_s$. The distances of the source and image locations from r_a are r_{sa} and r_{ia}, respectively:

$$r_{sa} = r_{ia} = r = \sqrt{(x-x_s)^2 + (y_s)^2} = \sqrt{(x-x_i)^2 + (y_i)^2}. \tag{9}$$

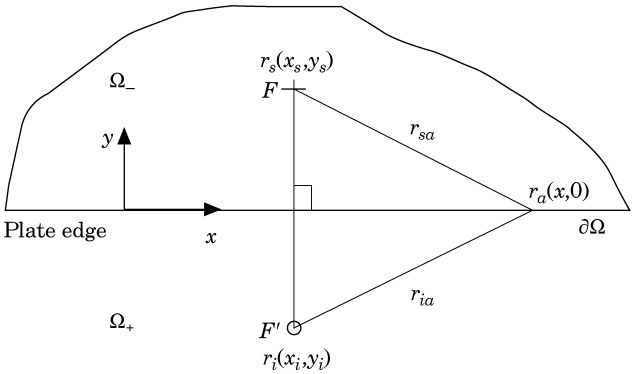

Figure 1. Imaging for semi-infinite plate.

The deflection u, normal slope θ, shear force F_y and the bending moment M_y at r_a can be obtained as the sum of the contributions from the source and the image. These are given by

$$u = -\frac{\mathrm{i}(F+F')}{8\lambda^2 D}\{[H_0^1(\lambda r) - H_0^1(\mathrm{i}\lambda r)]\}, \tag{10}$$

$$\theta = \frac{(F'-F)\mathrm{i}y_s}{8\lambda^2 Dr}\frac{\partial}{\partial r}[H_0^1(\lambda r) - H_0^1(\mathrm{i}\lambda r)], \tag{11}$$

$$Q_y = \frac{\mathrm{i}y_s(F'-F)}{8\lambda^2}\nabla^2\left(\frac{1}{r}\frac{\partial}{\partial r}[H_0^1(\lambda r) - H_0^1(\mathrm{i}\lambda r)]\right), \tag{12}$$

$$M_y = \frac{(F+F')}{8\lambda^2}\left\{\left\{\left(\frac{1}{r}-\frac{y_s^2}{r^3}\right)+\nu\left(\frac{1}{r}-\frac{x^2}{r^3}\right)\right\}\frac{\partial}{\partial r}+\left(\frac{y_s^2}{r^2}+\nu\frac{x^2}{r^2}\right)\frac{\partial^2}{\partial r^2}\right\}[H_0^1(\lambda r) - H_0^1(\mathrm{i}\lambda r)]. \tag{13}$$

If $F' = -F$, the deflection and bending moment along the edge become zero simultaneously, as equations (10) and (13) clearly indicate. This is nothing but the simply supported boundary condition along the edge. If $F' = F$, the plate will have the zero normal slope and the zero shear force along the edge as shown by equations (11) and (12). This is the second type of boundary condition, the roller boundary condition which can be realized by using the imaging technique. The free-free and clamped boundary conditions along the plate edge cannot be achieved by using simple image sources alone. For these boundary conditions, according to Chen [13], "the reflected wave has a local near field response which contains waves propagating along the edge of plate and evanescent in orthogonal directions". This type of behavior cannot be simulated by the point image source, irrespective of its strength. This *edge wave* is localized within a zone near the edge that becomes narrower as the frequency increases. So, at high frequencies, the free-free boundary condition may be approximated by the roller boundary condition (as demonstrated by the narrow beam example in section 4) and the clamped boundary condition may be approximated by the simply supported boundary condition [13].

3. APPLICATION TO A SIMPLY SUPPORTED RECTANGULAR PLATE

3.1. BOUNDARY CONDITIONS

Next, the results obtained for a semi-infinite plate are extended to a finite rectangular plate. In Figure 2, the four edges of the plate are denoted by E1, E2, E3 and E4, respectively. A '+' sign indicates a positive image and a '0' symbol represents a negative image. The strength of all the image sources is equal in magnitude to the applied force amplitude F. This configuration of source and images tends to satisfy the simply supported boundary conditions on the edges of the plate. To see how this is being done, consider the edge E2. The row of images R5 is the mirror image of R6. This is analogous to the case of the semi-infinite plate which has equal and opposite forces at the same distance on either side of the edge, to achieve the simply supported boundary condition. Therefore, their contributions to the deflection and bending moment along E2 get cancelled. The same is the case with R4 and R7. The only row of images which contributes to the deflection along E2 is R1. Similarly, R9 contributes to deflection on edge E4, V1 on edge E3 and V9 on edge E1. As more reflections are taken into account, the distance of the rows/columns contributing to displacement and bending moment from the corresponding edges increases

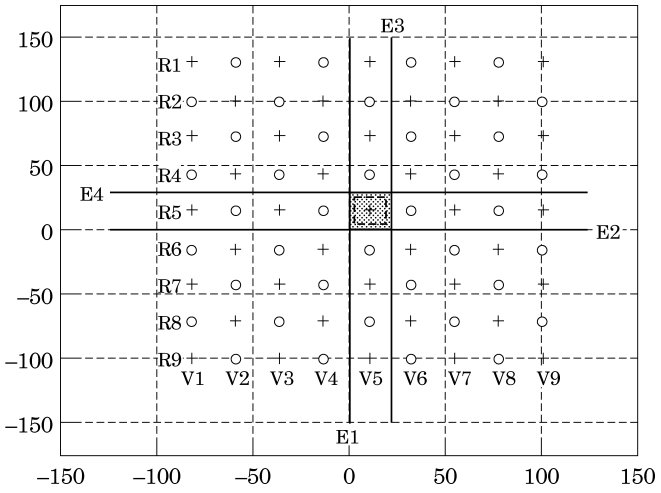

Figure 2. Infinite plate with positive (+) and negative (0) sources equivalent to simply supported plate with edges E1, E2, E3 and E4 excited at (x_s, y_s).

and the contribution decreases. In the limit, the boundary conditions on all the edges of the plate will be simply supported.

3.2. CONCENTRATED HARMONIC LOAD

For a concentrated harmonic load of amplitude F at the point $\check{r}_s(x_s, y_s)$, the steady state deflection at $\check{r}_0(x, y)$ is known exactly from the conventional modal analysis technique as

$$u(x, y) = \sum_{m=1}^{\infty} \sum_{n=1}^{\infty} B_{mn} \sin(m\pi x/a) \sin(n\pi y/b), \tag{14}$$

where

$$B_{mn} = \frac{4F \sin\left(\dfrac{m\pi x_s}{a}\right) \sin\left(\dfrac{n\pi y_s}{b}\right)}{\{ab[\bar{D}((m\pi/a)^2 + (n\pi/b)^2)^2 - \rho h\omega^2]\}}, \qquad \bar{D} = D(1 + i\eta). \tag{15}$$

Consider a rectangular steel plate example with simple supports on all four edges. The dimensions of the example plate considered are length $a = 0{\cdot}5842$ m along x, width $b = 0{\cdot}7366$ m along y and a thickness h of $0{\cdot}762$ mm. The loss factor for structural damping η is taken to be $0{\cdot}03$.

In Figure 3, the real (Re) and imaginary (Im) parts of the dynamic compliance $C(\omega) = (u/F)(\omega)$ are plotted as a function of x/a along $y/b = 0{\cdot}34$, when the load is applied at $\check{r}_s$ $(0{\cdot}65a, 0{\cdot}51b)$; the origin (0, 0) is at the bottom left corner of the plate. The frequency of excitation is $f = \omega/2\pi = 100$ Hz. The number of reflections (k) considered for the method of images is 40. There is an excellent agreement between the solutions obtained from both methods.

The cross-point dynamic compliance spectrum given $\check{r}_s$ at $(0{\cdot}65a, 0{\cdot}51b)$ at $\check{r}_0$ at $(0{\cdot}91a, 0{\cdot}96b)$ is plotted in Figure 4. The results from modal analysis and method of images with $(k = 40)$ are identical.

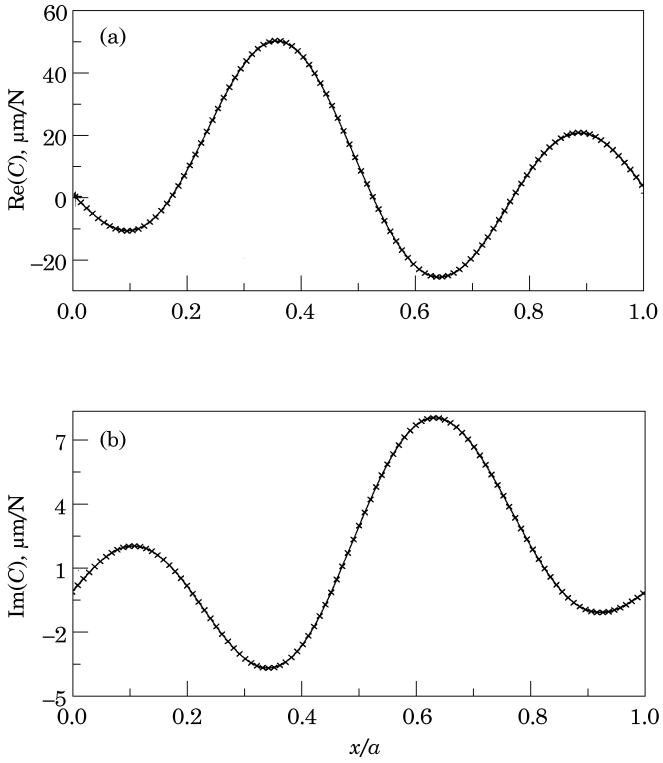

Figure 3. Dynamic compliance along the line $y/b = 0{\cdot}34$ due to unit force at $(0{\cdot}65a, 0{\cdot}51b)$. ×, Modal analysis; ——, method of images.

3.3. CONVERGENCE AND EFFECT OF DAMPING

Two error estimates e_1 and e_2 are defined as follows:

$$e_1 = \sqrt{\frac{\sum\limits_{g} (u_k - u_m)(\overline{u_k - u_m})}{\sum\limits_{g} (u_m)(\overline{u_m})}}, \qquad e_2 = \sqrt{\frac{\sum\limits_{bg} u_k \overline{u_k}}{\sum\limits_{bg} u_{k0} \overline{u_{k0}}}}, \tag{16, 17}$$

where the subscript g represents any grid point and the subscript bg denotes a grid point on the plate boundary, u_{k0} is the deflection due to the source alone, u_k is the deflection due to the source and images after k reflections, u_m is the exact solution for deflection obtained from modal analysis and the overbar implies complex conjugation. Therefore, e_1 is a measure of the deviation of the approximate solution obtained by the method of images from the exact solution and e_2 is a measure of convergence of the boundary conditions that must be satisfied. As the number of reflections (k) increases, if e_1 and e_2 approach zero, the solution obtained due to the method of images converges to the exact solution.

The loss factor η was reduced by an order of magnitude from 0·03 to 0·003 to study the effect of damping on the convergence rate of the solution. It was observed that a higher number of reflections is required for an accurate solution at the lower values of damping. This is evident from Figure 5 where the dynamic compliance variation along the line $x/a = 0{\cdot}87$ is plotted given a unit concentrated force at $(0{\cdot}65a, 0{\cdot}51b)$. The frequency of excitation is again 100 Hz. From this figure and other results, though not reported here,

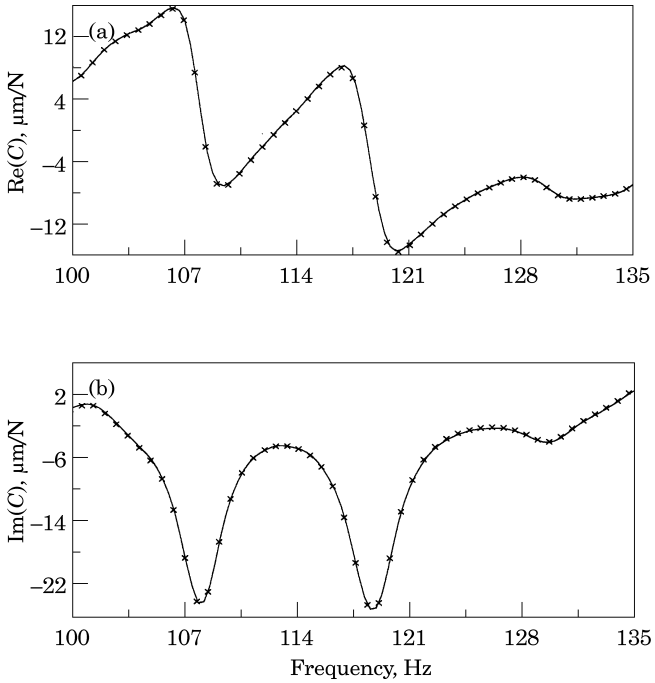

Figure 4. Dynamic compliance spectra between (0·91a, 0·96b) and (0·65a, 0·51b). ×, Modal analysis; ——, method of images.

it is clear that one must choose the k judiciously by considering various factors such as η and the frequency range of interest.

3.4. RECIPROCITY

The expression for the response at $\vec{r}_0$ due to a point load excitation at $\vec{r}_s$ obtained from modal superposition is given by equations (14) and (15). If we interchange the co-ordinates of the observation and the excitation locations, i.e. (x, y) and (x_s, y_s), we still obtain the same expression for the displacement. Hence, as expected, the reciprocity relationship holds. Similarly, the method of images also obeys reciprocity. But it is not transparent from the way the solution is obtained. If the source and the observation points are interchanged, the set of image locations obtained is completely different. It is interesting to find two entirely different series of Hankel functions add up to the same dynamic response. For the plate example chosen with $\omega = 100$ Hz, $\eta = 0{\cdot}03$ and $k = 50$, the results obtained by interchanging the source and the observation points are identical to nine decimal places as evident from Table 1.

3.5. DISTRIBUTED LOAD

For the same example, consider the load $F(\vec{r}_s)$ to be distributed over the surface of the plate. Assume it to be given by $F(x, y_s) = Fx/a$. For the method of images, the distributed force is replaced by an equivalent set of concentrated loads. The solution obtained is compared with the exact solution obtained from modal superposition which is still given by equation (14). But now

$$B_{mn} = \frac{4F(-1)^{m+1}\sin(n\pi y_s/b)}{\{bm\pi[\bar{D}((m\pi/a)^2+(n\pi/b)^2)^2-\rho h\omega^2]\}}. \tag{18}$$

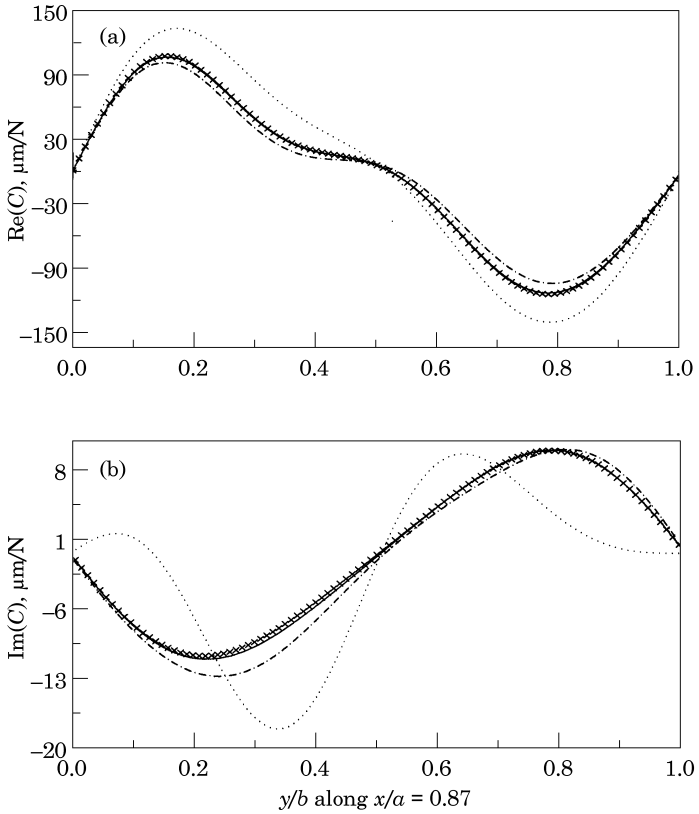

Figure 5. Dynamic compliance along $x/a = 0{\cdot}87$ due to unit force at $(0{\cdot}65a, 0{\cdot}51b)$. Loss factor η is 0·003. ×, modal analysis; . . . , method of images with 100 reflections; – · – · –, method of images with 200 reflections; ——, method of images with 400 reflections.

For the imaging technique, if the number of point loads is q, the strength of each source is given as

$$F(j) = \frac{F_0(j-1)a}{q(q-1)}, \qquad j = 1 \cdots q. \tag{19}$$

The sum of all the point harmonic loads is

$$\sum_{j=1}^{q} F(j) = F_0 a/2, \tag{20}$$

which is equal to the total force exerted by the distributed ramp load $F(\hat{r}_s)$.

Figure 6 presents plots of the forced harmonic response at 100 Hz due to a ramped load of $F = 100\ N/m$, given $y_s = 0{\cdot}69b$. The response is measured along the line $x/a = 0{\cdot}87$. The number of reflections considered for the method of images is 40. For the method of images, this distributed load is replaced by 100 point loads. Again, the results from the method of images and modal analysis match very well.

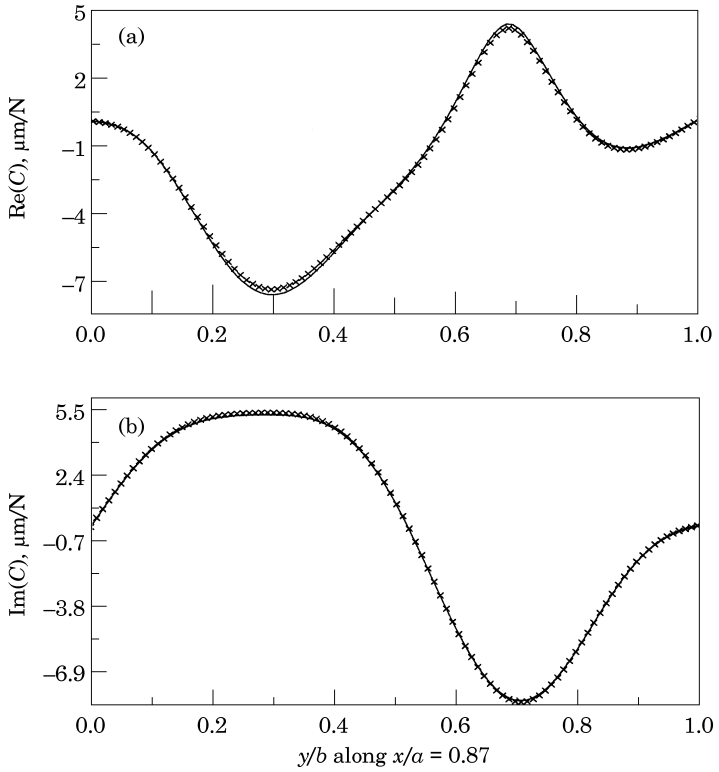

Figure 6. Real part of dynamic compliance along $x/a = 0{\cdot}87$ due to a ramp load of $F = 100$ N/m along $y/b = 0{\cdot}68$. ×, Modal analysis; ——, method of images.

4. APPLICATION TO SIMPLY SUPPORTED BEAMS

4.1. APPROACH I: NARROW PLATE CASE

The configuration of images shown in Figure 7 satisfies the roller boundary conditions on all the edges of the plate, i.e. along all the plate edges, the normal slope and shear force

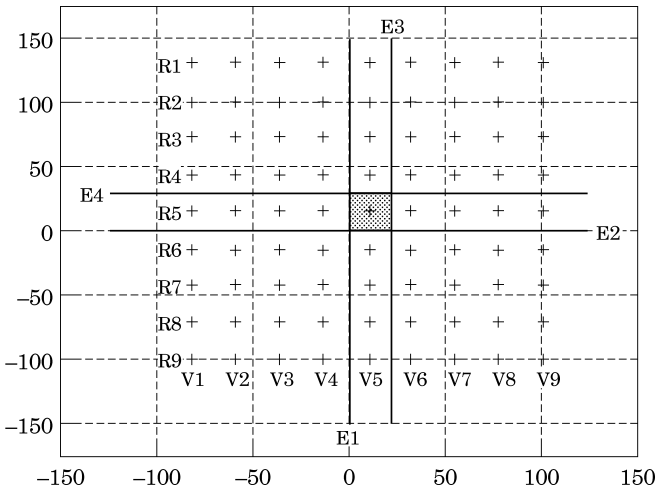

Figure 7. Infinite plate with source and image sources equivalent to a finite plate with roller boundary condition on all edges. Key as figure 2.

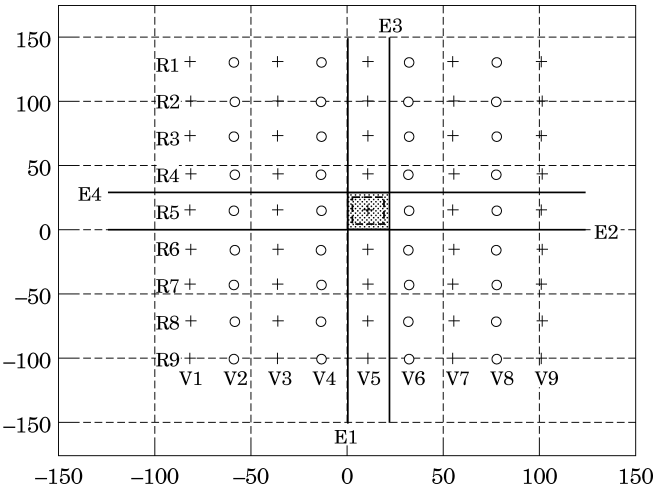

Figure 8. Edges E1 and E3 are simply supported and roller boundary conditions are satisfied along edges E2 and E4. Key as figure 2.

vanish. By choosing proper directions for the image sources, different boundary conditions can be obtained along each edge. Figure 8 shows an example where edges E1 and E3 are simply supported and edges E2 and E4 have roller boundary condition. This example is used to model a simply supported slender beam when $b/a \ll 1$. As in the case of a plate, we assume

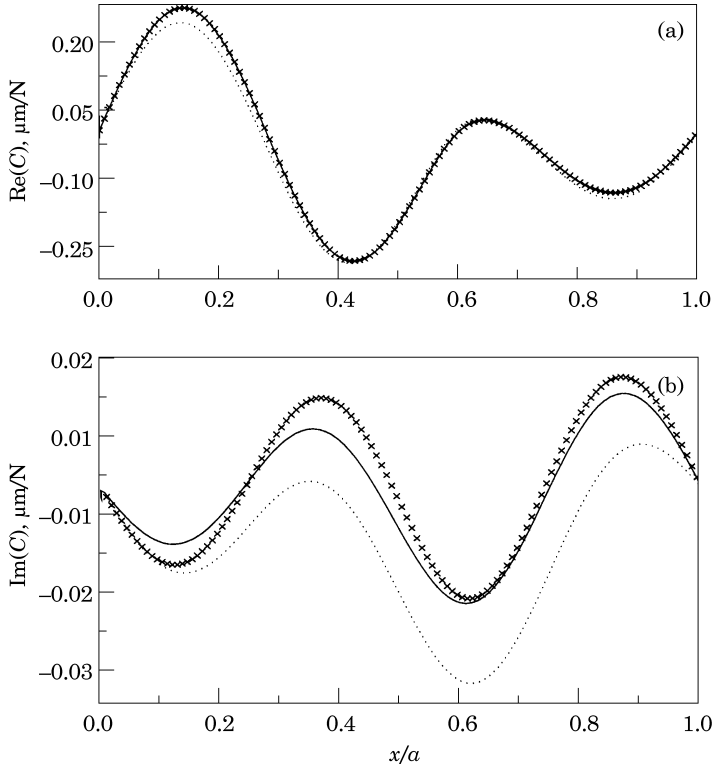

Figure 9. Dynamic compliance due to a unit concentrated load at $x/a = 0{\cdot}6$. Beam A modelled as a narrow plate. ×, Modal analysis; . . . , method of images with 100 reflections; ——, method of images with 400 reflections.

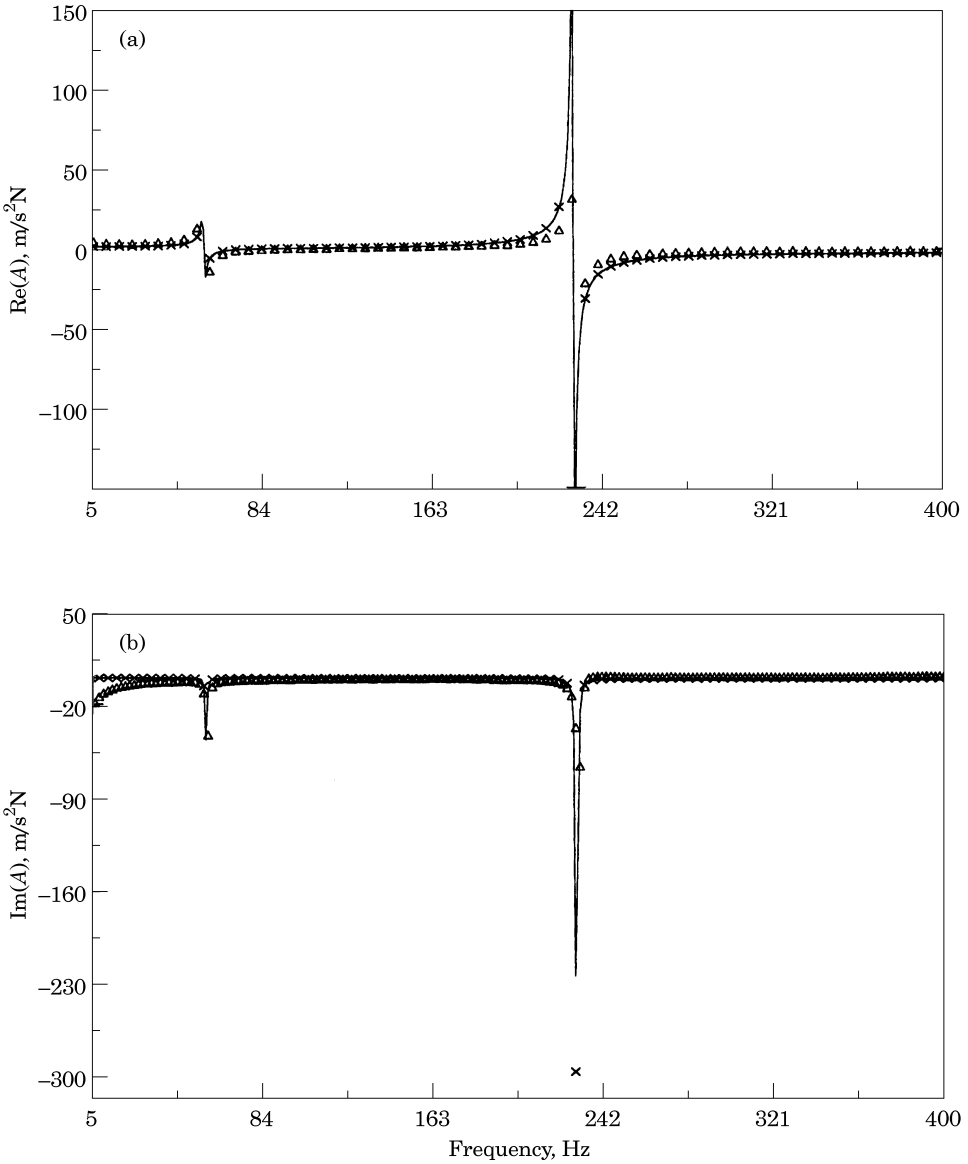

Figure 10. Acclerance spectra between 0·875a and 0·697a for beam B. – – –, method of images; ×, modal analysis; △, experiment.

the beam to be lightly damped. The Poisson ratio v is taken to be zero since the governing equation for transverse vibrations of a beam assumes no variation in deflection along the y-direction.

A steel beam of $a = 0{\cdot}381$ m, $b = 0{\cdot}0381$ m and $h = 4{\cdot}762$ mm, designated here as beam A, is considered. The loss factor η is 0·03. The dynamic compliance along the length of the beam due to a unit concentrated load at $x/a = 0{\cdot}6$ is plotted in Figure 9. The frequency of excitation is 1000 Hz. From the figure, it is observed that the solution from the method of images for a plate with mixed boundary conditions converges to the exact beam solution as k increases.

4.2. APPROACH II: BEAM FUNDAMENTAL SOLUTION

The governing equation for the transverse vibration of a beam is given in terms of displacement as

$$\frac{\partial^2}{\partial x^2}\left(EI\frac{\partial^2 w}{\partial x^2}\right)+\rho S\frac{\partial^2 w}{\partial t^2}=p(x,t). \tag{21}$$

If structural damping is taken into account, E in equation (21) can be replaced by $E(1+\mathrm{i}\eta)$. For the classical viscous damping case, the governing differential equation becomes

$$\frac{\partial^2}{\partial x^2}\left(EI\frac{\partial^2 w}{\partial x^2}\right)+c\frac{\partial w}{\partial t}+\rho S\frac{\partial^2 w}{\partial t^2}=p(x,t). \tag{22}$$

The following derivation of the beam fundamental solution is from Graff [14], but it has been modified to account for structural or viscous damping. Consider an infinite beam subjected to a harmonically varying, unit concentrated load placed at $x=x_s$. As in the case of a plate, the frequency parameter is given by $\lambda^4=\rho S\omega^2/EI(1+\mathrm{i}\eta)$ for structural damping and $\lambda^4=(\rho S\omega^2-\mathrm{i}c\omega)/EI$ for viscous damping. The four values of λ are

$$\lambda=\gamma-\mathrm{i}\beta, \qquad \beta+\mathrm{i}\gamma, \qquad -\gamma+\mathrm{i}\beta, \qquad -\beta-\mathrm{i}\gamma. \tag{23}$$

The fundamental solution for the infinite beam is given as

$$U(x)=\frac{\mathrm{i}}{E(1+\mathrm{i}\eta)I}\left\{\frac{1}{4(\gamma-\mathrm{i}\beta)^3}\exp(-\mathrm{i}(\gamma-\mathrm{i}\beta)(x-x_s))\right.$$

$$\left.+\frac{1}{4(-\beta-\mathrm{i}\gamma)^3}\exp(-\mathrm{i}(-\beta-\mathrm{i}\gamma)(x-x_s))\right\}, \qquad x>x_s, \tag{24}$$

$$U(x)=\frac{\mathrm{i}}{E(1+\mathrm{i}\eta)I}\left\{\frac{1}{4(\beta+\mathrm{i}\gamma)^3}\exp(-\mathrm{i}(\beta+\mathrm{i}\gamma)(x-x_s))\right.$$

$$\left.+\frac{1}{4(-\gamma+\mathrm{i}\beta)^3}\exp(-\mathrm{i}(-\gamma+\mathrm{i}\beta)(x-x_s))\right\}; \qquad x<x_s. \tag{25}$$

As in the case of a plate, a *simply supported* condition is obtained when the strength of the image force is equal and opposite to that of the applied force F. For a concentrated harmonic load F at the point $\bar{r}_s(x_s)$, the exact solution for deflection at the point $\bar{r}_0(x)$ is given from modal superposition as

$$u(x)=\sum_{m=1}^{\infty} B_m \sin(m\pi x/a), \tag{26}$$

where

$$B_m=\frac{2F\sin(m\pi x_s/a)}{a[E(1+\mathrm{i}\eta)I(m\pi/a)^4-\rho S\omega^2]}. \tag{27}$$

TABLE 1

Reciprocity check for the plate example at 100 *Hz*

$\vec{r}_0$	$\vec{r}_s$	Re(C)μm/N	Im(C)μm/N
(0·43a, 0·34b)	(0·78a, 0·76b)	−3·6678014934800393E-02	1·7432166043526748E-02
(0·78a, 0·76b)	(0·43a, 0·34b)	−3.6678014934799825E-02	1·7432166043526624E-02

An aluminum beam of $a = 0{\cdot}508$ m, $b = 0{\cdot}102$ m and $h = 6{\cdot}35$ mm, designated here as beam B, is considered. The accelerance spectrum between the points $0{\cdot}875a$ and $0{\cdot}697a$ is obtained from experiment. The viscous damping coefficient for modal analysis and the method of images is calculated in such a way that the first resonance peak matches with the experimental results. Here, c is taken to be 9 Ns/m^2. The critical damping, c_{c1}, for the first mode for a simply supported beam is given as $c_{c1} = 2\pi^2\sqrt{EI\rho S}/a^2$. c_{c1} for this beam is found to be 1225·13 Ns/m^2. the damping ratio ζ for this particular value of damping coefficient is $\zeta = c/c_{c1} = 0{\cdot}00717$. Figure 10 represents the accelerance spectra between the points $0{\cdot}875a$ and $0{\cdot}697a$. The frequency range is 5–400 Hz. It can be observed from Figure 10 that the results from the method of images match well with experimental and analytical modal analyses.

Even though both approaches yield the same response, the advantages of using the beam fundamental solution over the plate fundamental solutions are as follows. First, the problem becomes one-dimensional and its solution can be obtained much faster. Second, beams of arbitrary cross-section can be studied. If the beam is modelled as a narrow plate, we are restricted to plates of rectangular cross-section.

4.3. EIGENSOLUTIONS

The forced harmonic response data as calculated by the method of images can be used to find natural frequencies ω_r and mode shapes by using the coincident-quadrature technique commonly employed in experimental modal testing. For the sake of illustration, the two beams corresponding to the results described in sections 4.1. and 4.2. were analyzed. Natural frequencies predicted by the method of images exactly match with the measured data in Table 2. An attempt was made to simulate the simply supported boundary condition in the experiment, but only the first few modes can be realized.

5. BEHAVIOR AT HIGH FREQUENCY

At low frequency, the modes and the corresponding natural frequencies of structures are easily computed using the finite element method (FEM) and then the response using the normal mode expansion technique. At higher frequencies, the modal count increases

TABLE 2

Natural frequencies of beam A and beam B

Modal index m	Beam A		Beam B	
	Experiment	method of images	Experiment	method of images
1	77	77	59	59
2	304	304	230	230
3	688	688	—	545

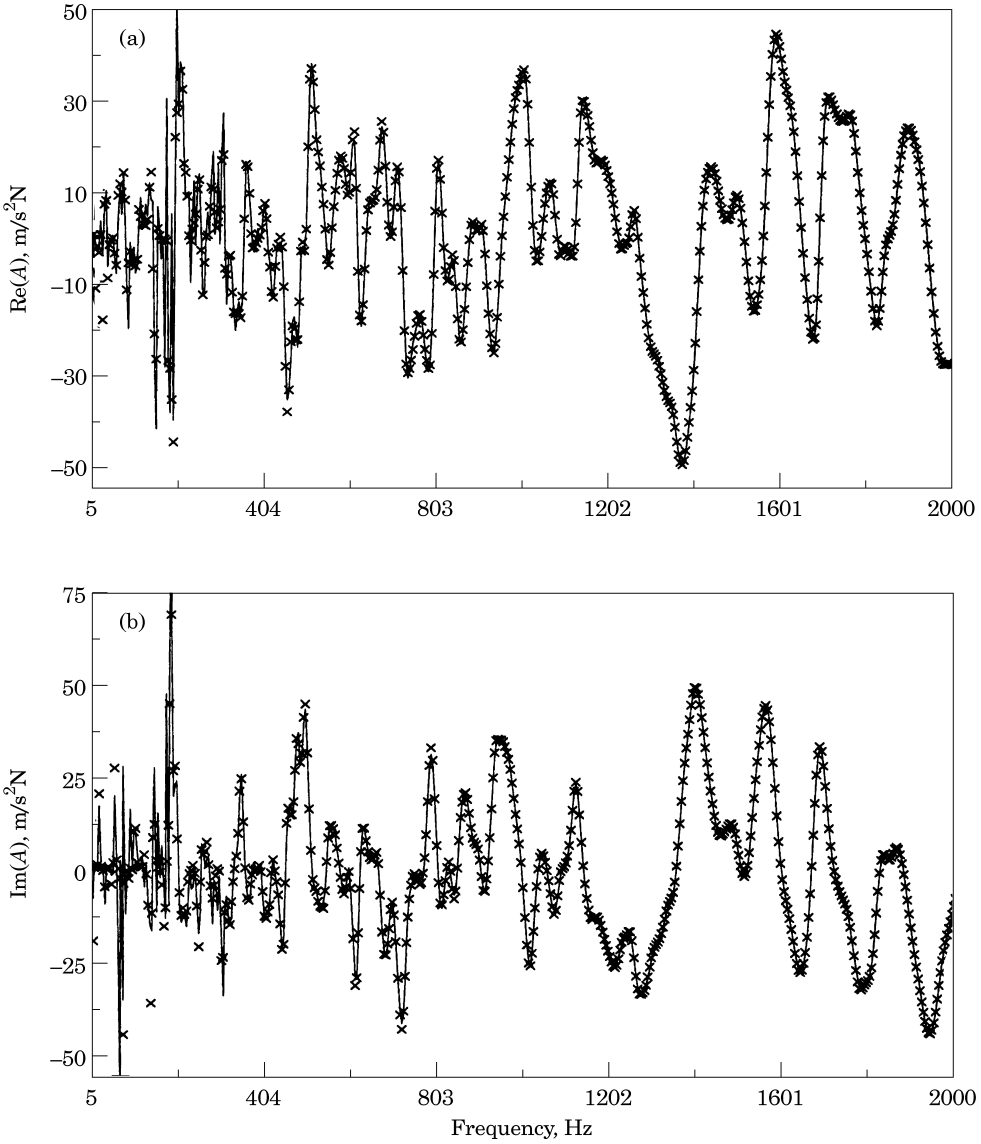

Figure 11. Accelerance spectra between (0·74*a*, 0·66*b*) and (0·30*a*, 0·38*b*). ×, Modal analysis; ——, method of images with five reflections.

significantly. Furthermore, to obtain accurate results, the finite element dimensions should be smaller than the wavelength of elastic waves at these frequencies. Thus, a very large finite element model is required which is not always practical or justifiable in terms of the computational expense involved and accuracy obtained. In contrast, the statistical energy analysis (SEA) method is more suitable at very high frequencies, but only spatially averaged band limited information is obtained. This approach also involves several simplifying assumptions and modelling criteria which are still being debated [15–17]. Asymptotic modal analysis has also been proposed as a viable analysis approach [17].

Using the method of images, we have observed that fewer reflections are needed to obtain the same accuracy at higher frequencies. In other words, for the same number of reflections, the accuracy increases with frequency. This behavior is a departure from that

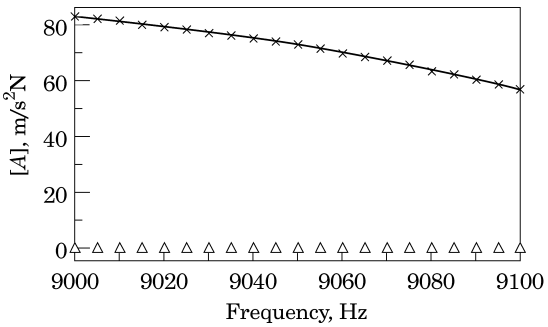

Figure 12. Accelerance spectra between $(0{\cdot}74a, 0{\cdot}66b)$ and $(0{\cdot}30a, 0{\cdot}38b)$. $\times$, Modal analysis; ——, method of images with five reflections; $\triangle$, FEM.

of the conventional methods such as the FEM whose accuracy reduces at higher frequencies. For the sake of illustration, again consider the rectangular plate example with simply supported boundary conditions, under a point harmonic load F at $\vec{r}_s(0{\cdot}03a, 0{\cdot}38b)$. The response point is fixed at $\vec{r}_o(0{\cdot}74a, 0{\cdot}66b)$ for all the calculations. For our method of images, the solution is calculated using only $k=5$ reflections, i.e. the deflection at any point is obtained by simply adding the contributions due to $(2\times 5+1)^2=121$ sources. A finite element model is constructed using 400 elastic shell elements [18]. Both predictions are compared with the exact modal analysis solutions over almost four decades of frequency from 1–10000 Hz. Over this range of frequencies, the natural frequencies are distributed as follows: 13 modes in the frequency range 0–100 Hz, 151 modes over 100–1000 Hz and 1595 modes over 1000–10 000 Hz. Two arbitrary frequency ranges, first at the low end from 5 to 2000 Hz and the second at the high end from 9000 to 9100 Hz are selected to compare the results. Given the wide range of frequencies, it is appropriate to choose the accelerance $A(w)=-u\omega^2/F$ as the sinusoidal transfer function in place of $C(w)$, where $-u\omega^2$ is the transverse acceleration of the plate.

Figure 11 shows the typical frequency response curves from 5 to 2000 Hz. In Figure 11, only the method of images is compared to the exact solution. Both are almost indistinguishable. Figure 12 shows the typical comparison at very high frequencies where 400 spectral points are distributed over 9000 to 9100 Hz. The method of images is again in excellent agreement with the exact solution but FEM fails to predict the response. Further, no clear cut resonances are seen. This is because high modal damping values are observed given a frequency-invariant loss factor of 0·03. It suggests that the asymptotic modal analysis or SEA type methods [15–17] might be suitable to predict this type of response. However,

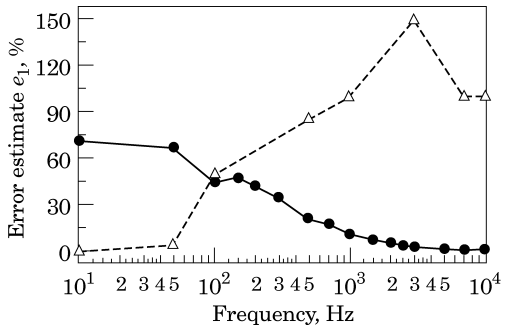

Figure 13. Convergence estimate e_1 versus frequency. —●—, Method of images with five reflections; – –△– –, FEM with 400 elements.

no *a priori* assumptions or procedures are needed in our method to find the band limited responses.

To better understand these results, the convergence estimate e_1 as given by equation (16) is plotted in Figure 13 for both methods with the exact modal solution as the benchmark. Even though either method could be made to yield improved behavior, if more reflections are chosen for the method of images or by decreasing the element size in FEM, certain trends are obvious. First, the FEM predictions are based on the eigensolutions which are prone to errors at the higher frequencies. Second, the method of images seems to improve its prediction capability as the frequency is increased. It is believed to be related to the image placement distance which depends on dimensions of the plate in relation to the elastic wavelength which becomes much smaller at higher frequencies. Finally, both methods show opposite trends over the spectral scale.

6. CONCLUSIONS

A new method of images has been developed for the harmonic analysis of plate and beam vibrations. Even though only a limited number of illustrative examples have been considered to verify the proposed procedure, certain observations can be made. Unlike the finite element method and other modal band methods, the solution accuracy of the method of images increases with an increase in the frequency and damping. Also, one can choose to analyze the response at just one location, unlike FEM where the solution has to be obtained at all the nodes. This procedure is in contrast to the modal methods where all the modes must be known *a priori* before the harmonic response can be calculated. The method of images seems very promising as a potential analysis tool because of its computational efficiency and accuracy in the medium and high frequency regimes. Work is proceeding along these directions and complicated plate shapes are being examined. However, more research is needed before it can be applied to practical structures and machines.

ACKNOWLEDGMENTS

This work has been supported by the U.S. Army research Office (URI Grant DAAL-03-92-G-0120; Project Monitor: Dr. T. L. Doligalski).

REFERENCES

1. A. D. Pierce 1989 *Acoustics–An Introduction to its Physical Principles and Applications*. New York: Acoustical Society of America.
2. G. L. James 1980 *Geometric Theory of Diffraction for Electromagnetic Waves*. London: Institution of Electrical Engineers.
3. S. H. Crandall and L. E. Wittig 1972 *Dynamic Response of Structures Symposium Proceedings* 55–71. Oxford: Pergamon.
4. S. H. Crandall 1977 *Stochastic Problems in Dynamics* (B. L. Clarkson editor) 366–389. London: Pitman.
5. S. H. Crandall 1979 *Developments in Statistics* Volume **2**, 1–82. New York: Academic Press. Random vibration of one and two-dimensional structures.
6. S. S. Lee 1976 *Ph.D. Dissertation*, *Massachusetts Institute of Technology*. Lanes of intensified response in structures excited by wide-band random excitation.
7. A. J. Langley and P. H. Taylor 1979 *International Journal of Engineering Science* **17**, 1039–1047. Chladni patterns in random vibration.
8. L. Cremer and M. Heckl 1988 *Structure-Borne Sound* (Translated and revised by E. E. Unger). Berlin: Springer-Verlag.
9. A. W. Leissa 1993 *Vibration of Plates*. New York: Acoustical Society of America.

10. D. E. Beskos 1991 *Boundary Element Analysis of Plates and Shells*. Berlin: Springer-Verlag.
11. Y. Niwa, S. Kobayashi and M. Kitahara 1981 *Theoretical and Applied Mechanics* **29**, 287–367. Eigen frequency analysis of a plate by the integral equation method.
12. A. Sommerfeld 1964 *Partial Differential Equations in Physics*. New York: Academic Press.
13. G. Chen, M. P. Coleman and J. Zhou 1991 *SIAM Journal on Applied Mathematics* **51**, 967–983. Analysis of vibration eigen frequencies of a thin plate by the Keller-Rubinow wave method: clamped boundary conditions with rectangular or circular geometry.
14. K. F. Graff 1991 *Wave Motion in Elastic Solids*. New York: Dover.
15. J. Woodhouse 1981 *Journal of the Acoustical Society of America* **69**, 1695–1709. An approach to the theoretical background of statistical energy analysis applied to structural vibration.
16. C. H. Hodges and J. Woodhouse 1986 *Reports on Progress in Physics* **49**, 107–170. Theories of noise and vibration in complex structures.
17. E. H. Dowell and Y. Kubota 1985 *Journal of Applied Mechanics* **52**, 949–957. Asymptotic modal analysis and statistical energy analysis of dynamical systems.
18. ANSYS 1992 *User's Manual*. Houston (PA): Swanson Analysis Systems, Inc.

APPENDIX A: LIST OF SYMBOLS

a	length
A	dynamic accelerance
B_{mn}	contribution to the displacement from m, n mode
b	width
c	coefficient of viscous damping
C	dynamic compliance
c_{c1}	critical damping coefficient for the first mode
D	flexural rigidity of the plate
$\bar{D}$	complex flexural rigidity
e_1, e_2	convergence estimates
E	Young's modulus
f	frequency (Hz)
F	strength of the source
F'	strength of the image
h	thickness
H_0^1	zero order Hankel function of the first kind
i	imaginary unit
I	area moment of inertia
Im	imaginary part of a complex quantity
k	number of reflections
m, n	modal indices
M_n	bending moment
M_t	twisting moment
M_y	bending moment along the edge
p	applied external force
Q_y	transverse shear force along the edge
q	number of point loads replacing the distributed force
r_a	a point on the edge of the semi-infinite plate
$\check{r}_o(x, y)$	position vector of the response point
$\check{r}_s(x_s, y_s)$	position vector of the excitation point
r_{sa}	distance between the source and observation points
r_{ia}	distance between the image and observation points
Re	real part of a complex quantity
S	cross-sectional area
t	time
u	displacement amplitude
u_k	deflection amplitude from method of Images
u_{k0}	deflection amplitude due to a single source alone
u_m	deflection amplitude from modal summation method
U	fundamental solution for an infinite plate or beam
V_n	shear force

w	transverse displacement
x, y	co-ordinates axes
α	angle between the x-axis and the outer normal
δ	Dirac delta function
$\partial\Omega$	boundary of the domain
η	loss factor for structural damping
λ	frequency parameter
∇^2	Laplacian operator
∇^4	biharmonic operator
ν	Poisson ratio
ω	angular frequency
Ω_-	interior of the domain
Ω_+	exterior of the domain
ρ	density
θ	normal slope

Superscripts

$^-$	complex conjugate
$^\rightarrow$	vector

Subscripts

bg	boundary grid point on convergence grid
g	grid point on the convergence grid